Journal of Cleaner Production 170 (2018) 1–13

Contents lists available at ScienceDirect

Journal of Cleaner Production

journal homepage: www.elsevier.com/locate/jclepro

Flowsheet-based model and exergy analysis of solid oxide electrolysis cells for clean hydrogen production

Karittha Im-orb [a], Nuttawut Visitdumrongkul [a], Dang Saebea [b], Yaneeporn Patcharavorachot [c], Amornchai Arpornwichanop [a, *]

[a] Computational Process Engineering Research Unit, Department of Chemical Engineering, Faculty of Engineering, Chulalongkorn University, Bangkok, 10330, Thailand
[b] Department of Chemical Engineering, Faculty of Engineering, Burapha University, Chonburi, 20131, Thailand
[c] School of Chemical Engineering, Faculty of Engineering, King Mongkut's Institute of Technology Ladkrabang, Bangkok, 10520, Thailand

ARTICLE INFO

Article history:
Received 21 January 2017
Received in revised form
4 September 2017
Accepted 13 September 2017
Available online 13 September 2017

Keywords:
Solid oxide electrolysis cell
Modeling
Energy
Exergy
Flowsheet simulation

ABSTRACT

A solid oxide electrolysis cell (SOEC) is an electrochemical technology used for hydrogen production via a steam electrolysis reaction. Because the existing SOEC models are complicated, the aim of this study is to develop a user-friendly SOEC model in a flowsheet simulator (Aspen Plus). The developed model is used to perform a parametric analysis to investigate the effects of key process parameters, i.e., operating temperature, current density, steam concentration, sweep gas type and number of cells, on the SOEC performance. The simulation results show that the voltage and the overall overpotential decrease as the cell temperature increases, whereas the opposite trends are observed when the current density increases. From the energy and exergy analyses, the total energy demand slightly increases with cell temperature, whereas the electrical energy demand decreases. Based on an operating temperature of 1273 K when the SOEC uses oxygen as the sweep gas, the highest energy and exergetic efficiencies of 78.45% and 92.20% are achieved at a current density of 2500 A m^{-2} and at a steam concentration of 90% in a 500-cell stack.

1. Introduction

Currently, fossil fuels (i.e., coal, natural gas, propane, gasoline and diesel) are not only used as a major source of energy production but are also used as a feedstock for many chemical synthesis processes. An increased energy demand causes an increase in fossil fuel consumption rate, and as a result, a large amount of greenhouse gases, which lead to global warming and public health issues, are emitted from the combustion unit (Mikulčić et al., 2016). Therefore, the production of energy from clean alternative resources, such as solar, wind and biomass has become an interesting topic. Although there are several technologies used to produce electricity from renewable sources, i.e., wind turbines and photovoltaic cells; the produced electricity is still inconsistent (Pozzo et al., 2015).

Hydrogen is regarded as an attractive sustainable energy carrier due to its eco-friendly and high energy density characteristics (Authayanun et al., 2013; Bayat et al., 2014; Valente et al., 2017). Among several hydrogen production processes, such as steam reforming, partial oxidation, autothermal reforming and gasification (Dutta, 2014; Fan et al., 2016), the steam reforming of natural gas is widely used; the derived product gas consists of hydrogen, carbon monoxide and carbon dioxide (Angeli et al., 2014). The gasification process, which converts carbonaceous substances into syngas, carbon dioxide, tar and sulfur dioxide via a thermochemical reaction, is also used for hydrogen production (Perna et al., 2016; Iribarren et al., 2014). Because fossil fuels are used as the main feedstock for steam reforming and gasification processes, the emission of greenhouse gases (e.g., carbon dioxide) occurs. Electrolysis technology, which is a clean technology, used to produce hydrogen by converting water or steam into hydrogen via electrochemical reactions, has been introduced and has received increasing attention (He et al., 2013; Kim et al., 2015).

Electrolysis technology or electrolysis cells, are categorized into three types, i.e., alkaline electrolysis cells (AECs), proton exchange membrane electrolysis cells (PEMECs) and solid oxide electrolysis cells (SOECs). AECs, which were the first fabricated type of

* Corresponding author.
E-mail address: Amornchai.A@chula.ac.th (A. Arpornwichanop).

http://dx.doi.org/10.1016/j.jclepro.2017.09.127
0959-6526/

electrolysis cell, are used to produce hydrogen at low temperature and pressure. The AEC electrolyte is a potassium hydroxide solution (KOH), which can corrode the cell electrode. A PEMEC is then introduced to operate at elevated pressure in the range of 30–60 bar without any additional compression unit. This technology uses a membrane to separate hydrogen and oxygen; therefore, high purity hydrogen (>99.99%) is achieved (Sun et al., 2014). However, the PEMEC requires a significant amount of electricity to operate, resulting in a high operating cost. The SOEC offers superior energy conversion efficiency compared with the other technologies. Because of the high operating temperature of the SOEC, which ranges from 800 to 1273 K, a special electrode material is required (Stempien et al., 2013). The SOEC seems to be a promising technology for hydrogen production due to its superior energy conversion efficiency; however, it is still in the research and development phases. Therefore, more studies are required to improve the SOEC performance from both technical and economic points of view (Millet and Grigoriev, 2013; Menon et al., 2014).

Currently, studies on SOECs mostly focus on the development of new electrode and electrolyte materials to reduce the electricity consumption and extend the cell lifetime. Some experiments were performed to develop new electrode materials (Mahmood et al., 2015; Palm et al., 2016). Shao et al. (2013) proposed Ni-YSZ-supported tubular solid oxide cells (SOCs), which were fabricated using a dip-coating and co-sintering method. The performances of the developed tubular SOCs were evaluated both in fuel cell and electrolysis modes. They found that the cell with a 3% pore-former exhibited the best performance in both SOFC and SOEC modes. Zhang et al. (2013) presented a new solar-driven high temperature steam electrolysis system for hydrogen production. The characteristics and electrical and thermal energy demands of their proposed process were investigated. Li et al. (2014) performed the experiment to investigate the hydrogen production efficiency based on the performance of a planar cathode-supported SOEC with 1-cell, 2-cell and 30-cell electrolysis stacks. The SOECs were tested at an operating temperature of 1073 K for 500 h. A maximum efficiency of 52.7% was achieved in the 30-cell stack.

Modeling of SOECs is another approach used in the preliminary design of the SOEC process. It is also used as a tool to investigate the influence of the change in operating parameters on the process performance. Ni et al. (2007) studied the effects of the process configurations and operating parameters on the SOEC performance. The suitable configuration was an anode-supported SOEC, and the optimum process condition was achieved at an operating temperature of 1273 K and at a steam mole fraction of 0.6. Udagawa et al. (2008) developed a one-dimensional dynamic model of a cathode-supported planar intermediate temperature SOEC stack with air flow introduced through the cells. Their developed model was used to study the steady state behavior of the SOEC and the prospect for stack temperature control by varying the air flow rate. Currently, the published SOEC models are complicated, especially when integrated with other process models. Therefore, the development of a user-friendly SOEC model is an important topic. To cope with this issue, a well-developed flowsheet simulation software, such as Aspen Plus, is selected. The flowsheet simulation software contains various built-in basic unit operation modules, such as a reactor, separator and mixer. Moreover, a rigorous thermodynamic and physical property database coupled with additional computational tools, such as a mathematical block, optimization scheme and design specifications, are also included; therefore, the development of new process model can be more easily accomplished (Zhang et al., 2005).

Because the SOEC involves an endothermic process that requires some external energy, an energy analysis should be performed to design an efficient SOEC system. However, the use of an energy term to evaluate the benefit of sustainable energy systems may be insufficient; an exergy analysis, which considers the irreversible increase in entropy, was therefore introduced to clearly identify the efficiency improvement and the reduction in thermodynamic loss of the green technologies (Hajjaji et al., 2012).

The objective of this study is to develop a user-friendly SOEC model using Aspen Plus. An electrochemical model coded in FORTRAN language is also included and used to determine the electrical characteristics of the SOEC. The developed SOEC model is used to investigate the effects of operating parameters, such as cell temperature, operating current density, steam concentration, number of cells and sweep gas type, on the SOEC performance. In addition, energy and exergy analyses are performed to determine the operating condition that offers the best performance.

2. Model of solid oxide electrolysis cell

The solid oxide electrolysis cell (SOEC) consists of an electrolyte, a cathode and an anode, which are normally fabricated from yttria-stabilized zirconia cermet (YSZ), Ni-yttria-stabilized zirconia cermet (Ni-YSZ) and lanthanum strontium manganite-YSZ (LSM-YSZ), respectively (Millet and Grigoriev, 2013). The planar configuration of the SOEC is illustrated in Fig. 1. The electrochemical reactions involved in the SOEC are summarized in Table 1. The steam is fed to a porous cathode. When the electricity is supplied, the steam moves to the cathode-electrolyte interface, and it is reduced to form pure hydrogen and oxygen ions. The hydrogen gas then diffuses back up through the cathode, and it is collected at the cathode surface as hydrogen fuel, while the oxygen ions migrate through the electrolyte to the anode. At the electrolyte-anode interface, the oxygen ions are oxidized to form pure oxygen gas, which is collected at the surface of the anode and displaced by the supplied sweep gas.

The SOEC model is developed using Aspen Plus, and the model flowsheet is shown in Fig. 2. Because the SOEC requires both electrical and thermal energy to carry out the electrochemical reactions, the electrical energy (represented by stream POWER) and the thermal energy (represented by stream QE) are supplied to the SOEC. The overpotential heat is represented as QOVP, and the heat required at the anode channel is represented as QA.

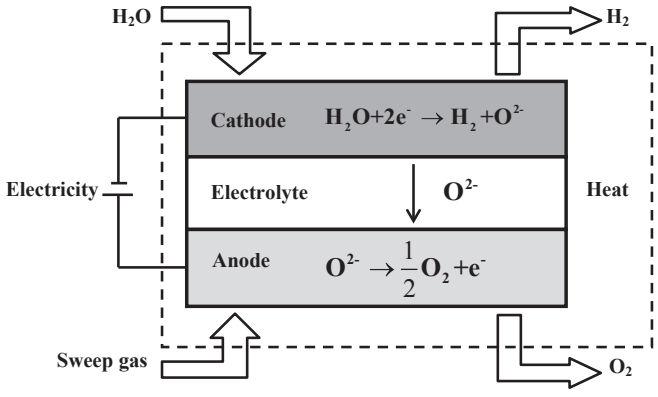

Fig. 1. The planar configuration of the SOEC.

Table 1
Electrochemical reactions that occurred in the SOEC.

Cathode	$H_2O + 2e^- \rightarrow H_2 + O^{2-}$
Anode	$O^{2-} \rightarrow 0.5O_2 + 2e^-$
Overall reaction	$H_2O \rightarrow H_2 + 0.5O_2$

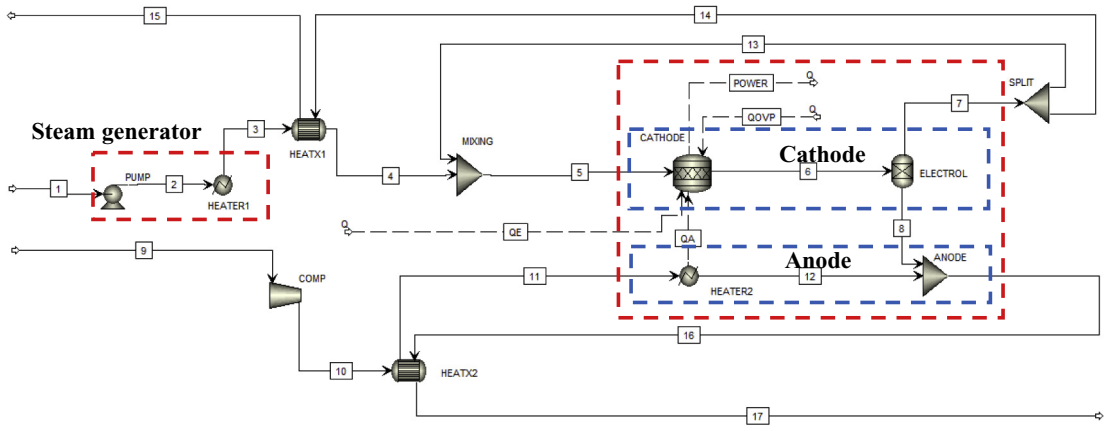

Fig. 2. SOEC flowsheet simulation (solid lines and dashed lines represent material streams and energy streams, respectively).

The steam (stream 4) is first mixed with hydrogen gas, which is recycled from the cathode channel (stream 13) to prevent nickel oxidation on the cathode, prior to being fed to the cathode. The RSTOIC reactor, represented as CATHODE, is used to simulate the electrochemical reaction of the steam at a specified reaction temperature. The thermal energy required for the reaction can be calculated by specifying the utilization factor of this reaction as a design spec. The product leaving the cathode channel is separated at the splitter block, which is represented as SPLIT. The splitting ratio is calculated and varied until the feed specification, which has a desired steam to hydrogen ratio of 0.1–0.9, is achieved. The cathode product consisting of hydrogen and oxygen is separated by an electrolyte, which is simulated using a separator block, referred to as ELECTROL. The oxygen totally permeates into the anode channel. The sweep gas (stream 9) is introduced to displace the oxygen from the anode channel. Moreover, it is used as a heating medium to convey heat between the cathode and the anode. The sweep gas is heated to the cathode temperature at a heater block, referred to as HEATER2, and then it is mixed with oxygen at the ANODE mixer block before leaving the anode. The thermal energy required for sweep gas preheating is represented as the stream QA.

The electrical energy required in SOEC is calculated using a mathematical model, which is coded in a calculator block using FORTRAN language. The required electrical energy consists of the equilibrium voltage and the overpotential. The equilibrium voltage, the minimum electrical energy required to carry out the reaction, can be calculated from Equations (1) and (2).

$$E = E^0 + \frac{RT}{2F}\ln\left(\frac{P_{H_2}P_{O_2}^{1/2}}{P_{H_2O}}\right) \tag{1}$$

$$E^0 = 1.253 - 2.4516\cdot10^{-4}T \tag{2}$$

where E is the equilibrium voltage (V), E^0 is the standard potential (V), R is the universal gas constant (8.3145 J mol^{-1} K^{-1}), T is the cell temperature (K), F is Faraday's constant (96,485 C mol^{-1}), and P_{H_2}, P_{O_2} and P_{H_2O} are the partial pressures of hydrogen, oxygen and steam (kPa), respectively.

The SOEC overpotential, the electrical energy loss, consists of the activation, the ohmic and the concentration overpotentials. The activation overpotential (η_{act}), which is the energy loss due to the chemical kinetics of the electrochemical reactions, can be calculated from Equations (3) and (4), which are derived from the Butler-Volmer equation.

$$\eta_{act,i} = \frac{RT}{F}\ln\left[\frac{J}{2J_{0,i}} + \sqrt{\left(\frac{J}{2J_{0,i}}\right)^2 + 1}\right] \tag{3}$$

$$J_{0,i} = \gamma_i \exp\left(-\frac{E_{act,i}}{RT}\right) \tag{4}$$

where J is the current density (A m^{-2}), $J_{0,i}$ is the exchange current density at the cathode (i = c) and anode (i = a) (A m^{-2}), γ_i is the pre-exponential factor of the cathode and anode (A m^{-2}), and $E_{act,i}$ is the activation energy of the cathode and anode (J mol^{-1} K^{-1}).

The ohmic overpotential (η_{ohm}), which is the loss due to a resistance within the electrolyte layer, can be calculated from Equation (5).

$$\eta_{ohm} = 2.99\cdot10^5 JL\exp\left(\frac{10300}{T}\right) \tag{5}$$

where L is the thickness of the electrolyte (m).

The concentration overpotential (η_{conc}) is caused by the mass transfer resistance between the electrode and electrolyte. This overpotential can be calculated using Equations (6) and (7), respectively.

$$\eta_{conc,c} = \frac{RT}{2F}\ln\left[\frac{\left(P_{H_2} + JRTd_c/2FD_{H_2O}^{eff}\right)P_{H_2O}}{\left(P_{H_2O} - JRTd_c/2FD_{H_2O}^{eff}\right)P_{H_2}}\right] \tag{6}$$

$$\eta_{conc,a} = \frac{RT}{4F}\ln\left(\frac{\sqrt{(P_{O_2})^2 + (JRT\mu d_a/2FB_g)}}{P_{O_2}}\right) \tag{7}$$

where d_c and d_a are the thicknesses of the cathode and anode (m), respectively, $D_{H_2O}^{eff}$ is the effective diffusion coefficient of steam (m^2 s^{-1}), μ is the dynamic viscosity of oxygen (kg m^{-1} s^{-1}), and B_g is the flow permeability (m^2).

The cathode concentration overpotential involves the reactant diffusion at the cathode. There are several diffusion models, i.e., Fick's model, the Duty gas model and the Stefan-Maxwell model. Because Fick's model is a non-complicated model and it can effectively describe gas transport, it is used in this study (Equation (8)) (Ni et al., 2006).

$$\frac{1}{D_{H_2O}^{eff}} = \frac{\xi}{n}\left(\frac{1}{D_{H_2-H_2O}} + \frac{1}{D_{H_2O,k}}\right) \quad (8)$$

The Knudsen diffusion ($D_{H_2O,k}$) and the molecular diffusion ($D_{H_2-H_2O}$) coefficients ($m^2\ s^{-1}$) can be calculated from Equations (9–14):

$$D_{H_2O,k} = \frac{4}{3} r \sqrt{\frac{8RT}{\pi M_{H_2O}}} \quad (9)$$

$$D_{H_2-H_2O} = 0.00133\left(\frac{1}{M_{H_2}} + \frac{1}{M_{H_2O}}\right)^{1/2} \frac{T^{3/2}}{P\sigma_{H_2-H_2O}^2 \Omega_D} \quad (10)$$

$$\sigma_{H_2-H_2O} = \frac{\sigma_{H_2} + \sigma_{H_2O}}{2} \quad (11)$$

$$\Omega_D = \frac{1.06036}{(T^*)^{0.1561}} + \frac{0.193}{\exp(0.47635T^*)} + \frac{1.03587}{\exp(1.52996T^*)} + \frac{1.76474}{\exp(3.89411T^*)} \quad (12)$$

$$T^* = \frac{T}{\varepsilon_{H_2-H_2O}/\kappa} \quad (13)$$

$$\frac{\varepsilon_{H_2-H_2O}}{\kappa} = \sqrt{\frac{\varepsilon_{H_2}}{\kappa}\frac{\varepsilon_{H_2O}}{\kappa}} \quad (14)$$

where ξ is the electrode tortuosity (−), n is the electrode porosity (−), r is the average electrode pore radius (m), M_{H_2O} and M_{H_2} are the molar masses of steam and hydrogen ($g\ mol^{-1}$), respectively, P is the operating pressure (kPa), σ_{H_2O} and σ_{H_2} are the collision diameters of steam and hydrogen (m), Ω_D is the dimensionless diffusion collision integral, T^* is the dimensionless temperature, and $\frac{\varepsilon_{H_2O}}{\kappa}$ and $\frac{\varepsilon_{H_2}}{\kappa}$ are the Lennard-Jones potentials of steam and hydrogen (K), respectively (Reid et al., 1987).

The permeability and dynamic viscosity used to calculate the anode concentration overpotential are derived from Equations (15) - (17) (Todd and Young, 2002).

$$B_g = \frac{n^3}{72\xi(1-n)^2}(2r)^2 \quad (15)$$

$$\mu = -1.692 + 889.75\tau - 892.79\tau^2 + 905.98\tau^3 - 598.36\tau^4 + 221.64\tau^5 - 34.75\tau^6 \quad (16)$$

$$\tau = \frac{T}{1000} \quad (17)$$

The cell potential of the SOEC is the sum of the equilibrium voltage (E) and all of the overpotentials as shown in Equation (18). The electrical current, a theoretical electrical current based on a specified utilization factor (U_f), can be calculated from Equation (19). It is noted that the utilization factor is defined as a ratio of the molar flow rate of steam used to produce hydrogen to that of the steam feed. The electrical current and cell area are used to calculate the current density from Equation (20). Normally, the current density is controlled in the range of 1000–3000 A m^{-2} to prevent SOEC electrode deterioration. The electrical power required for the SOEC operation is determined from Equation (21).

$$V = E + \eta_{conc,c} + \eta_{conc,a} + \eta_{act,c} + \eta_{act,a} + \eta_{ohm} \quad (18)$$

$$I = \frac{n_e U_f F \dot{N}_{H_2O} A}{N_{cell}} \quad (19)$$

$$J = \frac{I}{A} \quad (20)$$

$$W = IVN_{cell} \quad (21)$$

where V is the cell voltage (V), U_f is the utilization factor (−), $\dot{N}_{H_2O}$ is the molar flow rate of the steam feed ($mol\ s^{-1}$), A is the cell area (m^2), I is the electrical current (A), W is the power (W), and N_{cell} is the number of cells within the SOEC.

The energy efficiency of the SOEC is calculated from Equation (22). The overpotential heat, which is related to the overall overpotential, the current density and the cell area, can be determined from Equation (23),

$$\eta_{en} = \frac{\dot{N}_{H_2,out} LHV}{W + Q_{ovp}} \quad (22)$$

$$Q_{ovp} = \left(\eta_{conc,c} + \eta_{conc,a} + \eta_{act,c} + \eta_{act,a} + \eta_{ohm}\right) JAN_{cell} \quad (23)$$

where $\dot{N}_{H_2,out}$ is the molar flow rate of the hydrogen product ($mol\ s^{-1}$), LHV is the lower heating value ($J\ mol^{-1}$), and Q_{ovp} is the overpotential heat (W).

The total energy required for the SOEC operation (Q_T) consists of electrical and thermal energy. As the supplied electrical energy decreases, the supplied thermal energy should be increased to maintain the overall energy consumption. The net thermal energy required for SOEC operation can be calculated from Equation (24). The energy balance of the SOEC is shown in Equation (25). When the heat loss is considered to be negligible, the energy balance equation is therefore derived to be Equation (26).

$$Q_T = Q_r - Q_{ovp} - Q_{swg} - Q_E \quad (24)$$

$$Q_T - Q_{loss} + W_{elec} = 0 \quad (25)$$

$$Q_T + W_{elec} = 0 \quad (26)$$

where Q_r is the heat required for the reaction (W), Q_{swg} is the sweep gas heat (W), Q_E is the external heat (W), Q_{loss} is the energy loss (W), and W_{elec} is the SOEC electrical power (W).

The developed SOEC model is first validated with the experimental data reported by Momma et al. (1997) who investigated the J-V characteristics of hydrogen production by electrolyte-supported planar SOSE discs. The electrolyte, cathode, and anode are made from yttria-stabilized zirconia (YSZ), nickel–YSZ (Ni–YSZ) and a mixture of YSZ and strontium-doped lanthanum (LSM–YSZ), respectively. The thickness of the electrolyte, anode, and cathode are 1000, 100 and 100 μm, respectively. The SOEC is operated at a constant pressure of 100 kPa, steam mole fraction of 0.6 and operating temperature ranging from 1173 to 1273 K. The model input parameters are summarized in Table 2. A comparison of the flowsheet-based model predictions and experimental results of the SOEC is summarized in Table 3. The predicted cell voltages at different operating temperatures and current densities are in good agreement with the experimental results with the relative error ranging from 0 to 12.31%.

Table 2
Input parameters and operating conditions.

Operating temperature, T (K)	1273
Operating pressure, P (kPa)	506.5
Steam concentration (%)	90
Pre-exponential factor for anode exchange current density, γ_a (A m^{-2})	$2.051 \cdot 10^9$
Pre-exponential factor for cathode exchange current density, γ_c (A m^{-2})	$1.344 \cdot 10^{10}$
Activation energy for the anode, $E_{act,a}$ (J mol^{-1})	$1.2 \cdot 10^5$
Activation energy for the cathode, $E_{act,c}$ (J mol^{-1})	$1.0 \cdot 10^5$
Current density, J (A m^{-2})	2500
Electrode porosity, n	0.4
Electrode tortuosity, ξ	5.0
Average pore radius, r (μm)	0.5
Cell area, A (m^2)	0.04
Number of cells, N_{cell} (cell)	500
Sweep gas type	Oxygen
Anode support	
Electrolyte thickness, L (μm)	50
Cathode thickness, d_c (μm)	50
Anode thickness, d_a (μm)	500

3. Exergy analysis

Exergy is defined as the maximum amount of work that can be produced by a stream of matter, heat or work of the system as it comes to equilibrium with a reference environment (a reference state is represented by temperature T_0 and pressure P_0) (Dincer and Rosen, 2012). Unlike energy, exergy is not subject to the conservation law (except for ideal processes). Exergy is consumed or destroyed due to non-idealities or irreversibilities in any real processes. The present study assumes that the SOEC is operated under steady state and isothermal conditions; therefore, the exergy destruction, which is recognized as an important parameter indicating the efficiency of an energy process, is calculated from the exergy balance (Equation (27)).

$$\sum_{j=1}^{nQ} \dot{E}x_{Q,j} + \sum_{j=1}^{np} \dot{n}_j ex_j - \sum_{j=1}^{nr} \dot{n}_j ex_j + \dot{E}x_w - \dot{E}x_d = 0 \quad (27)$$

where $\dot{E}x_Q$ is the exergy of thermal energy (W), $\dot{n}$ is the molar flow rate (mol s^{-1}), ex is the specific exergies (J mol^{-1}), $\dot{E}x_w$ is the exergy of work (W), $\dot{E}x_d$ is the exergy destruction (W), and nQ, np and nr represent the number of heat streams, inlet streams, and outlet streams, respectively.

The relation between the exergy of thermal energy, which represents the quality of thermal energy, and the heat required for the system at a given temperature is shown in Equation (28) (Gundersen, 2009).

$$\dot{E}x_Q = \left(1 - \frac{T_0}{T}\right) Q \quad (28)$$

Table 4
Standard molar chemical exergy of selected substances at the reference state (T_0 = 298.15 K, P_0 = 101.325 kPa) (Szargut et al., 1988).

Substance	Chemical exergy (kJ mol^{-1})
H_2	236.09
H_2O (l)	0.90
H_2O (g)	9.50
O_2	3.97
CH_4	831.20
CO_2	19.48
CO	274.71
N_2	0.72

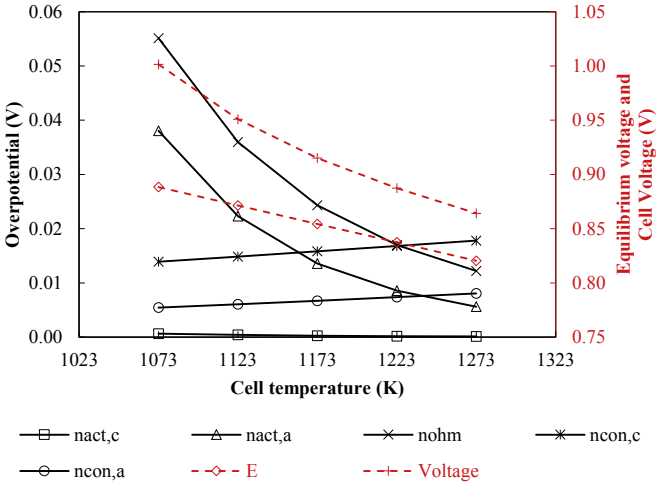

Fig. 3. Effect of operating temperature on the equilibrium voltage and overpotentials.

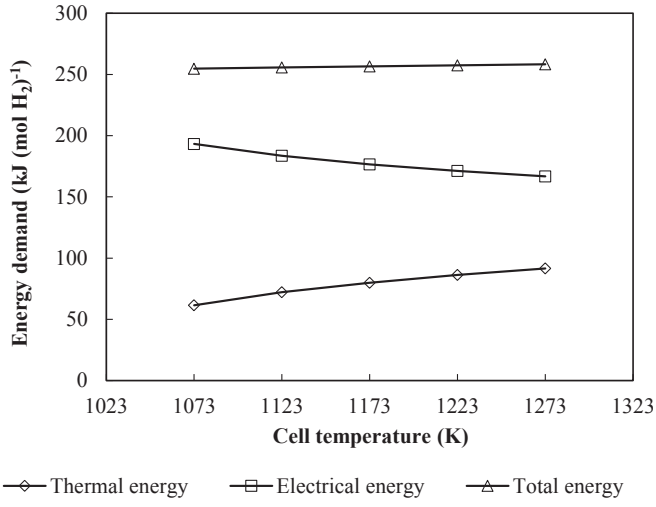

Fig. 4. Effect of operating temperature on the energy demand.

Table 3
Comparison between the flowsheet-based model predictions and experimental results.

Current density (A m^{-2})	Cell voltage at selected operating temperature (V)								
	1173 K			1223 K			1273 K		
	Exp.	model	Relative Error (%)	Exp.	model	Relative Error (%)	Exp.	model	Relative Error (%)
0	0.89	0.88	1.12	0.88	0.88	0.00	0.88	0.88	0.00
1000	1.15	1.121	2.52	1.194	1.047	12.31	0.98	0.994	1.43
2000	1.45	1.328	8.41	1.27	1.194	5.98	1.11	1.102	0.72
3000	1.65	1.534	7.03	1.45	1.339	7.66	1.23	1.208	1.79
4000	1.79	1.79	0.00	1.57	1.484	5.48	1.35	1.313	2.74

where T_0 is the reference temperature (K), and Q is the heat required for the system (W).

The specific exergy, which is a sum of the specific physical and chemical exergies, can be calculated from Equation (29) (Ghannadzadeh et al., 2012).

$$ex = ex_{ph} + ex_{ch} \tag{29}$$

where ex_{ph} is the specific physical exergy (J mol^{-1}), and ex_{ch} is the specific chemical exergy (J mol^{-1}).

The specific physical exergy (Equation (30)) is the maximum useful work obtained by passing the unit of mass of a substance of the considered state (T, P) to the environmental state (T_0, P_0).

$$ex_{ph} = (h - h_0) - T_0(s - s_0) \tag{30}$$

where h and h_0 are the enthalpies at the considered and reference environmental states (J mol^{-1}), respectively, and s and s_0 are the entropies at the considered and reference environmental states (J mol^{-1} K^{-1}), respectively.

The specific chemical exergy (Equation (31)) is the maximum useful energy obtained by passing from the environmental state to the dead state via chemical processes with reactants and products at the environmental temperature and pressure. The standard molar chemical exergies of selected substances at the reference state (T_0 = 298.15 K, P_0 = 101.325 kPa) are summarized in Table 4 (Szargut et al., 1988).

$$ex_{ch} = \sum y_i ex_{ch,i0} + RT_0 \sum y_i \ln y_i \tag{31}$$

where y_j is the content of component i, and $ex_{ch,i0}$ is the standard chemical exergy of component i (J mol^{-1}).

The exergy of work (Equation (32)) is the work done by the system, e.g., electrical and mechanical works, excluding the work due to the volume change.

$$\dot{E}x_w = \dot{W} \tag{32}$$

where $\dot{W}$ is the shaft work (W).

In the analysis, the exergetic efficiency, which is defined based on the inlet exergy ($\dot{E}x_{in}$) and the exergy destruction ($\dot{E}x_d$), can be calculated from Equation (33).

$$\eta_{ex} = 1 - \frac{\dot{E}x_d}{\dot{E}x_{in}} \tag{33}$$

where η_{ex} is the exergetic efficiency (−).

The exergy analysis provides the exergy destruction of each unit in the considered process with its magnitude indicating the inefficiency of energy utilization. The irreversibility is equivalent to the exergy destruction, and the value of the exergy destruction term is always positive in the real process due to the entropy generation.

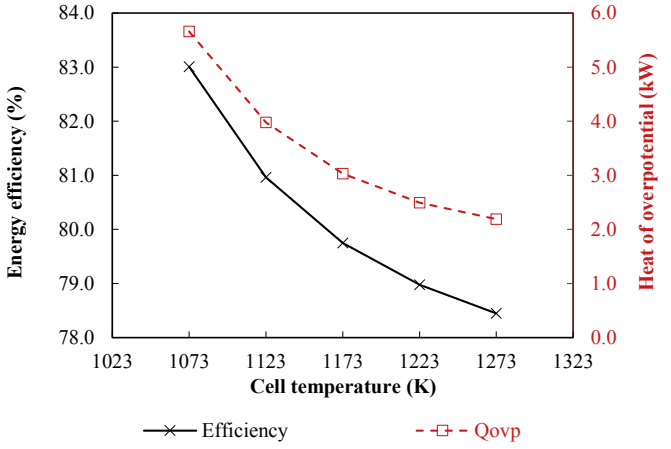

Fig. 5. Effect of the operating temperature on the energy efficiency and overpotential heat.

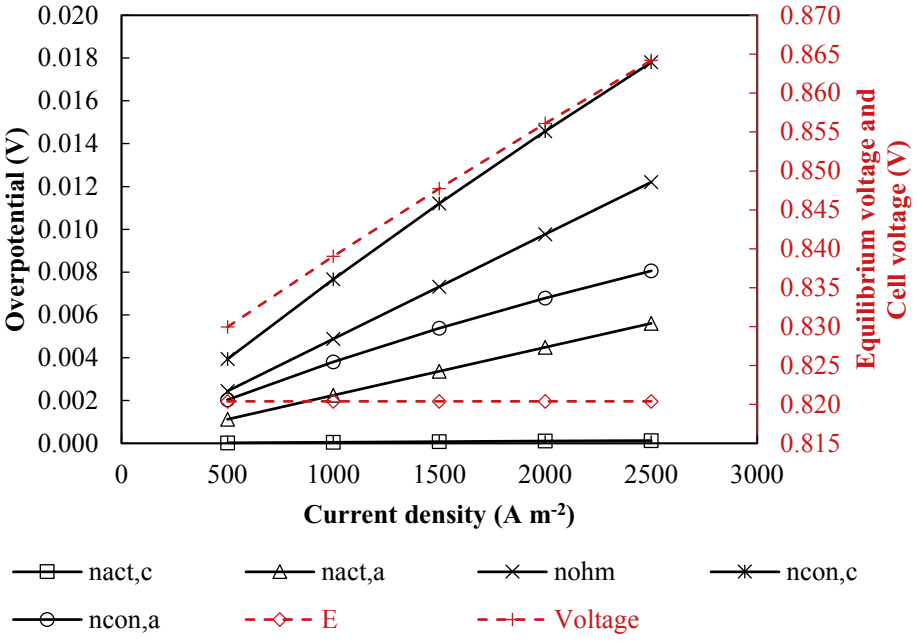

Fig. 6. Effect of the current density on the equilibrium voltage and overpotentials.

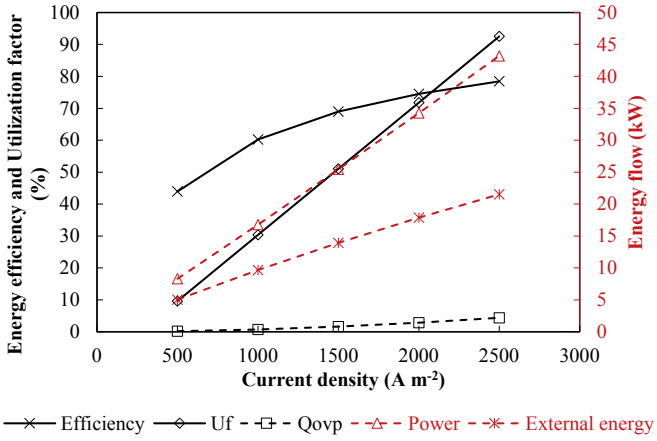

Fig. 7. Effect of the current density on the energy efficiency, utilization factor, overpotential heat, electrical power and external heat of the SOEC.

4. Results and discussion

4.1. Performance of solid oxide electrolysis cell

4.1.1. Effect of operating temperature

The effects of the operating temperature on the equilibrium voltage, overpotential, energy demand, energy efficiency and overpotential heat are investigated by varying the operating temperature in the range of 1073–1273 K. The variations in equilibrium voltage and individual overpotential are shown in Fig. 3.

When the electrochemical reaction rate and oxygen ion conductivity of the electrolyte increase when the operating temperature increases, a decrease in the activation overpotential is observed. The ohmic overpotential, the resistance of ionic conductivity in the electrolyte layer, dominates the cell potential. The ohmic overpotential decreases with the cell temperature due to significant increases in oxygen ion conductivity. Inversely, the concentration overpotential increases with temperature due to the increased steam effective diffusion coefficient, which indicates an increase in molar diffusion rate. As a result, the mass transfer resistance between the electrode and electrolyte increases.

The value of ohmic overpotential is much higher than that of the other overpotentials; therefore, the effect of operating temperature on the overall potential shows the same trend as that of the ohmic overpotential. Regarding the energy demand, the total energy demand slightly increases with the cell temperature, whereas the electrical energy demand decreases due to the increase in thermal energy demand (Fig. 4). This result is consistent with the previous study of Balta et al. (2016). Moreover, the energy efficiency of the SOEC slightly decreases due to the decrease in overpotential heat and electrical energy (Fig. 5).

4.1.2. Effect of current density

The current density is another parameter that affects the SOEC performance. The effect of current density on the SOEC performance is investigated by varying the current density in the range of 500–2500 A m^{-2} at a constant temperature of 1273 K. It is determined that all overpotentials increase with current density, as shown in Fig. 6. The cathode concentration overpotential shows the highest value; therefore, it dominates the cell overpotential. As shown in Fig. 6, the equilibrium voltage does not depend on the current density as shown in the Nernst equation (Equation (1)). The increase in cell voltage as the current density increases indicates that more electrical energy is required for the SOEC. As the overall overpotential increases with current density, the overpotential heat shows the same trend. Moreover, the utilization factor also increases with current density due to an increase in hydrogen production rate and SOEC energy efficiency (Fig. 7). Because the current density related to the supplied electrical energy, the selection of operating current density should consider the cost of electrical energy and the number of cells required to produce the desired amount of hydrogen product. For the SOEC with oxygen sweep gas operated at 1273 K, a maximum energy efficiency of 78.45% is found when the current density is maintained at 2500 A m^{-2}.

4.1.3. Effect of steam concentration

The effects of the steam concentration, which is the percentage

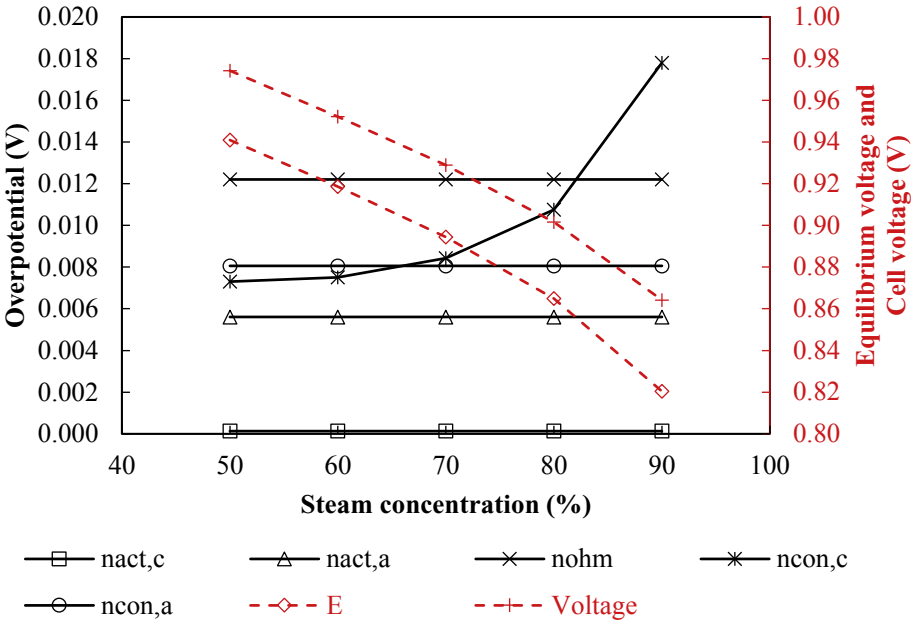

Fig. 8. Effect of steam concentration on the equilibrium voltage, overpotentials and cell voltage.

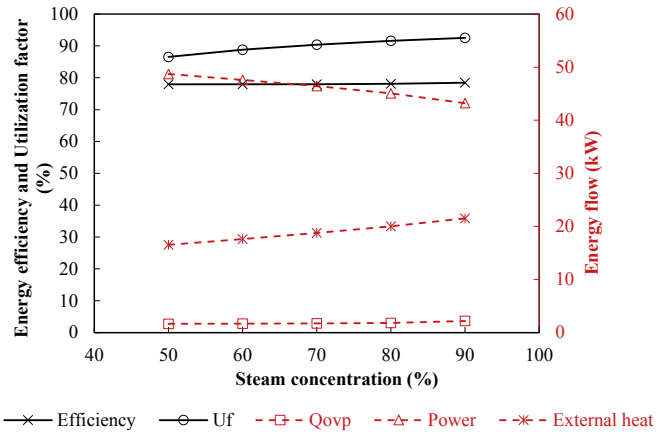

Fig. 9. Effect of steam concentration on the energy efficiency, utilization factor, overpotential heat, electrical power and external heat of the SOEC.

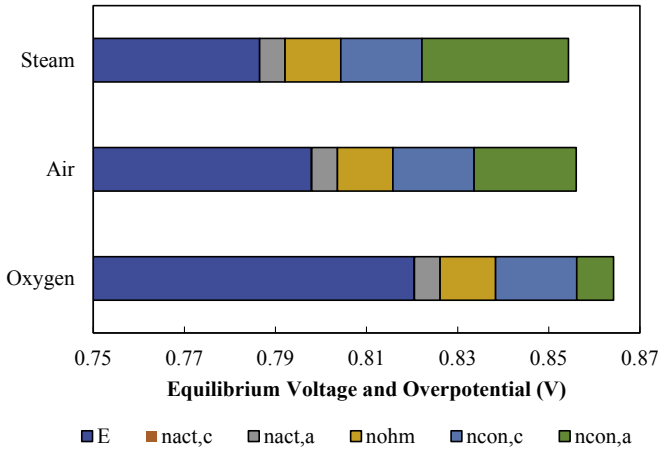

Fig. 10. Effect of the sweep gas type on the equilibrium voltage and overpotential.

of steam in the feed stream of SOEC, on the equilibrium voltage, overpotentials and cell voltage are also investigated by setting the cell temperature and current density at 1273 K and 2500 A m^{-2}, respectively. The steam concentration is then varied in the range of 50–90%. Fig. 8 shows that the equilibrium voltage decreases when the steam concentration increases due to an increase in steam partial pressure. The finding can be explained by the Nernst equation (Equation (1)). This result also shows the same trend as that found in the reported literature (Ni et al., 2006). The increase in steam concentration only affects the cathode concentration overpotential. The cathode concentration overpotential increases when the concentration of steam increases due to an increase in the molar diffusion rate in the cathode channel, resulting in an increase in the mass transfer resistance within the cathode. However, the increasing rate of cathode concentration is lower than the decreasing rate of the equilibrium voltage. Therefore, the increase in steam concentration causes the cell voltage and electrical energy to decrease, as shown in Fig. 8. To balance the energy consumption in the SOEC, more external thermal energy is required when the electrical energy decreases (Fig. 9). In this study, the steam concentration is adjusted by varying the recycle fraction of the product leaving the cathode, which contains hydrogen and unconverted steam. Moreover, the utilization factor increases as the steam concentration increases; however, the amount of produced hydrogen remained constant due to the lower amount of steam entering the cathode. A high steam concentration offers a high energy efficiency for the SOEC due to the decrease in electrical energy demand. As a result, a low operating cost is also achieved under these conditions.

4.1.4. *Effect of sweep gas type*

A sweep gas is used to displace or sweep the accumulated oxygen at the anode channel. The effect of the sweep gas type on the SOEC performance is investigated in this study. Due to the abundance and inexpensiveness, oxygen, air and steam are used as the sweep gases. The variations in the equilibrium voltage and overpotentials with the type of sweep gas are shown in Fig. 10. Because

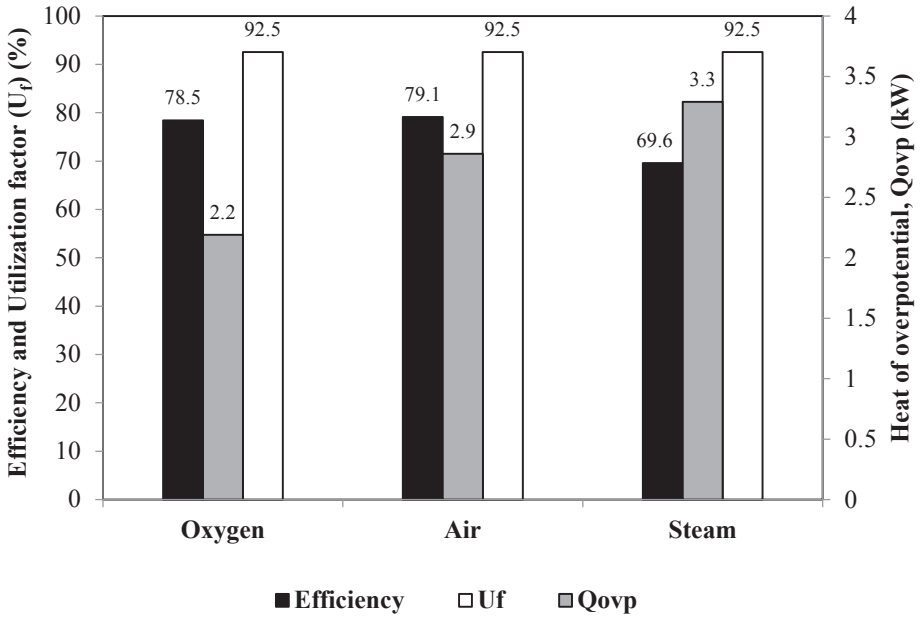

Fig. 11. Effect of the sweep gas type on the energy efficiency, utilization factor and overpotential heat.

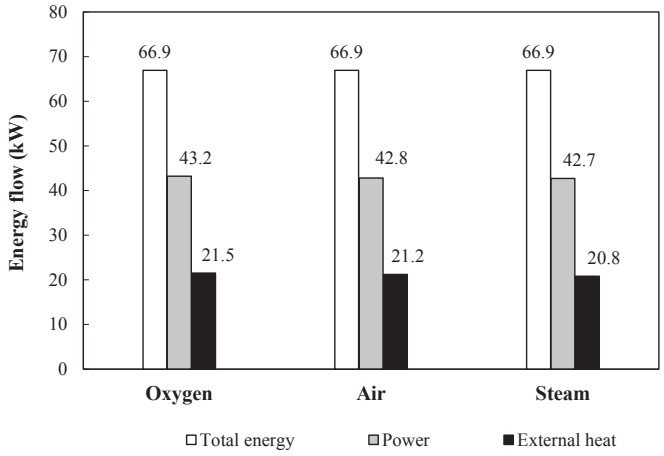

Fig. 12. Effect of the sweep gas type on the total energy, electrical power and external heat of the SOEC.

the equilibrium voltage depends on the partial pressure of oxygen, the highest equilibrium voltage is achieved when oxygen is used as the sweep gas. The use of air or steam as a sweep gas causes the oxygen partial pressure to decrease due to a N_2 dilution effect, resulting in a decrease in the equilibrium voltage. Inversely, the lowest overpotential is achieved when oxygen is used; as a result, the lowest overpotential heat is observed, and the highest energy efficiency is achieved (Fig. 11). Comparing with oxygen and steam, the use of air as a sweep gas offers the highest energy efficiency (Fig. 11). However, a dilution of pure oxygen produced with nitrogen is found. The variations in total energy, electrical and thermal energy demand are also investigated. As shown from Fig. 12, the lowest amount of thermal and electrical energy demand is achieved when steam is used as the sweep gas. The produced oxygen could be easily separated from the SOEC outlet stream, which contains oxygen and steam, by decreasing the temperature until the steam is totally condensed.

4.1.5. Effect of the number of cells

The effect of the number of cells on the SOEC performance is investigated by varying the number of cells in the range of 100–500. Fig. 13 shows that an increase in the number of cells do not significantly affect the overpotential heat. However, the amount of required electrical energy increases when the number of cells increases. The utilization factor increases when the number of cells increases due to the increase in the electrochemical reaction rate. Therefore, more external heat is required to carry out the reaction. Moreover, an increase of energy efficiency with the number of cells is also found; this result shows the same trend as that found in the reported literature (Li et al., 2014). However, to determine the optimum number of cells offering the highest SOEC performance, an economic evaluation should be further performed. For the SOEC with the oxygen sweep gas operated at 1273 K, a maximum energy efficiency of 78.45% is achieved in the 500-cell stack.

4.2. Exergetic performance of solid oxide electrolysis cell

4.2.1. Effect of operating temperature and current density

The effects of the operating temperature and current density on the exergy destruction and exergetic efficiency are investigated. At a constant steam concentration of 90% and with the number of cells at 500, the operating temperature and current density are varied in the range of 1073–1273 K and at 2000–2500 A m^{-2}, respectively. Fig. 14 shows that the exergy destruction increases with the operating temperature, whereas the exergetic efficiency decreases due to the increase in irreversibility. This implies that the energy utilization of a SOEC operating at a high temperature is not efficient. The effect of current density on the exergy destruction and exergetic efficiency exhibits the opposite trend as the operating temperature. A low exergy destruction and high exergetic efficiency can be achieved at a high operating current density and a low cell temperature.

4.2.2. Effect of the number of cells and steam concentration

The effects of the number of cells and the steam concentration on the exergy destruction and exergetic efficiency are also investigated by setting the operating temperature at 1273 K. The number

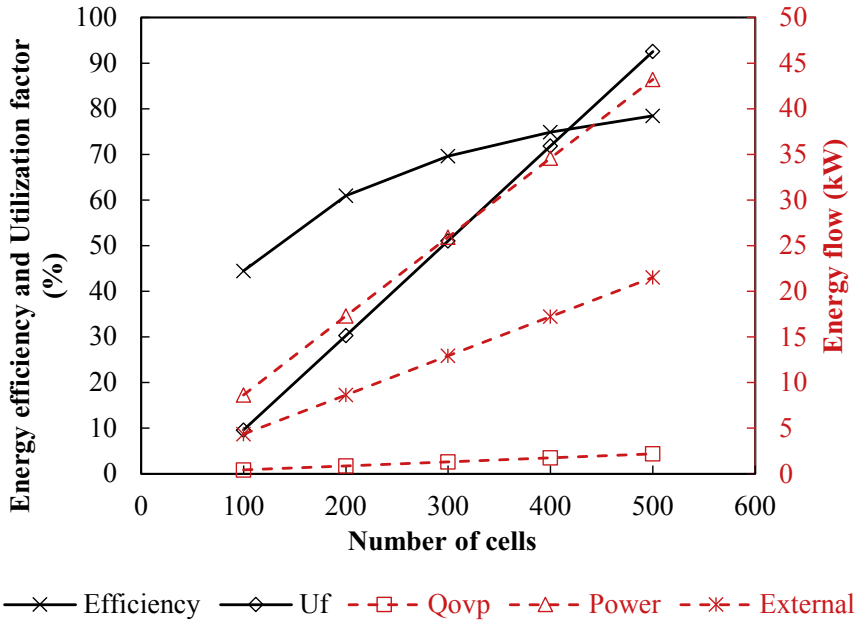

Fig. 13. Effect of the number of cells on the energy efficiency, utilization factor, overpotential heat, electrical power and external heat of the SOEC.

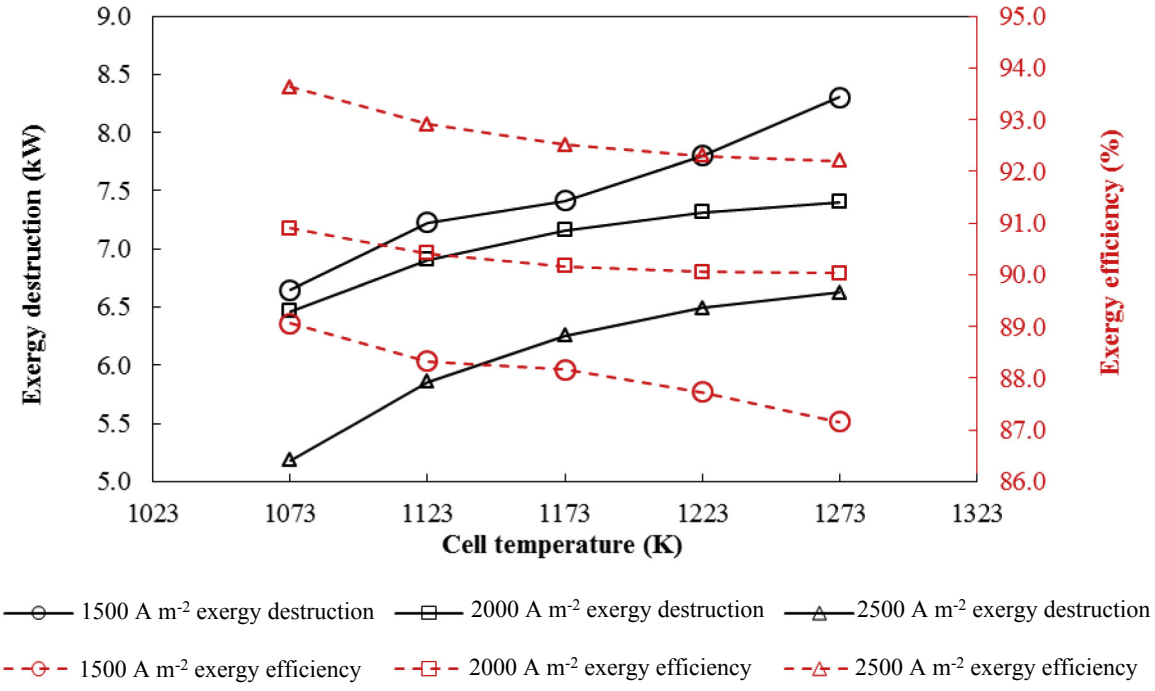

Fig. 14. Effect of the operating temperature and current density on the exergy destruction and exergetic efficiency.

of cells and the steam concentration are varied in the range of 200–500 and 80–90%, respectively. As shown in Fig. 15, the exergy destruction decreases as the number of cells increases. As the hydrogen production rate increases when the number of cells increases, a decrease in the exergy destruction and an increase in the exergetic efficiency can be observed. The same effect is found when the steam concentration is considered as a key parameter. As the concentration of steam in the feed increases, the concentration of steam in the recycled stream also increases, whereas the utilization factor decreases, resulting in a decrease in hydrogen production rate. Moreover, the increase in steam concentration causes the equilibrium voltage and the electrical energy demand to decrease. As a result, a decrease in exergy destruction and an increase in exergetic efficiency are observed.

4.2.3. Effect of the sweep gas type

The effects of the sweep gas type on the exergy destruction and exergetic efficiency are presented in this study. Oxygen, air and

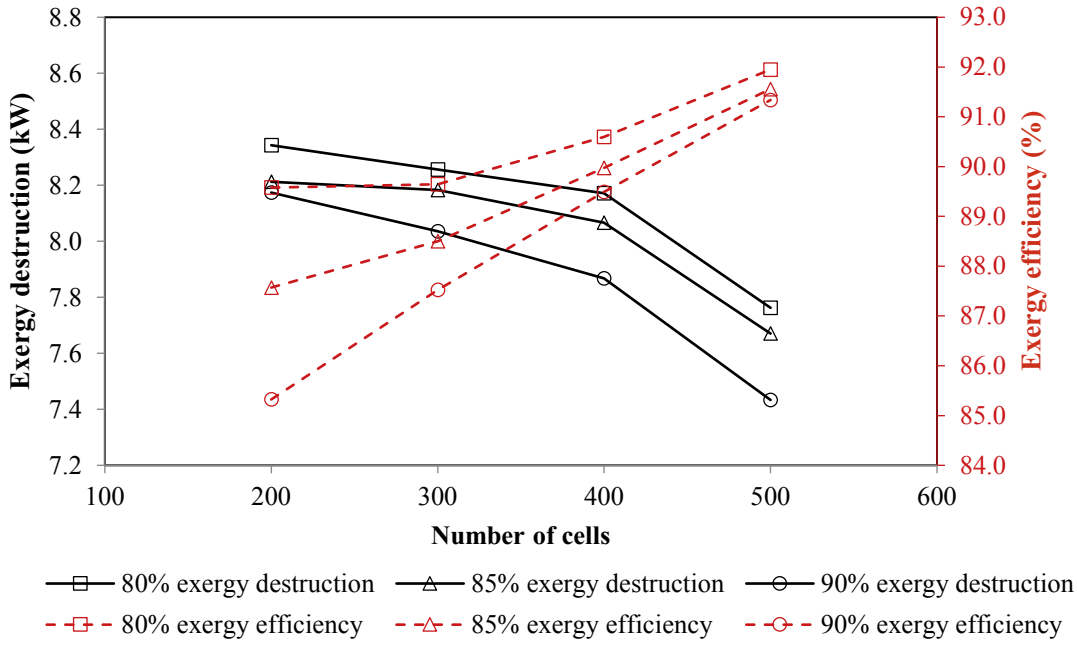

Fig. 15. Effect of the number of cells and steam concentration on the exergy destruction and exergetic efficiency.

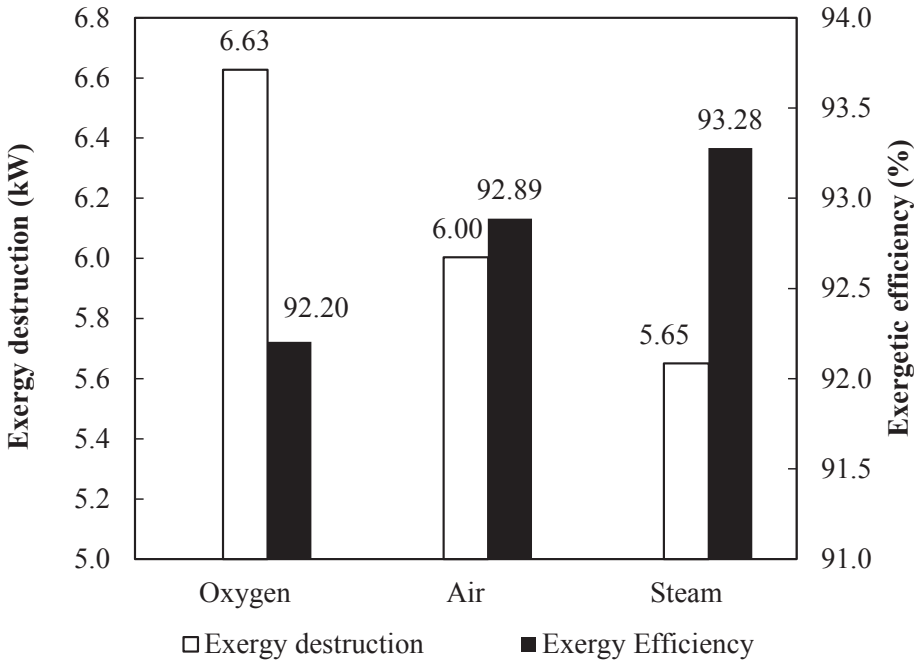

Fig. 16. Effect of the sweep gas type on the exergy destruction and exergetic efficiency.

steam are the considered sweep gases. Fig. 16 shows that the use of steam causes a decrease in the cell potential; therefore, the lowest exergy destruction is achieved. The highest exergy destruction is found when oxygen is used. Regarding the exergetic efficiency, as shown in Fig. 16, the exergetic efficiency of the SOEC system using different types of sweep gas exhibits the opposite trend as the exergy destruction.

Most of the energy and exergetic efficiencies derived from this study (ranging from 87 to 93%) are slightly higher than those (energy and exergetic efficiencies of 87% and 88%, respectively) reported by Balta et al. (2016) due to the use of a higher steam concentration and higher operating temperature. However, these values are very consistent with the practical efficiencies reported in the previous work. Based on a SOEC operating temperature of 1273 K, the highest energy and exergetic efficiencies of 78.45% and 92.20% are achieved at a current density of 2500 A m^{-2}, a steam concentration of 90% and with the number of cells at 500 when oxygen is used as the sweep gas.

5. Conclusions

A user-friendly model of an anode support planar SOEC was established using Aspen Plus. The developed flowsheet-based model shows a good prediction performance at high temperature compared with the reported mathematical model. The effects of changes in the operating parameters on the SOEC performance were investigated. The results indicate that the voltage and overall overpotential decrease with an increase in cell temperature due to a decrease in ohmic and activation overpotentials, which play an important role in the overall overpotential. The concentration overpotential is relatively negligible at low temperatures. The SOEC feed with high steam concentration is preferred due to the reduction in equilibrium voltage and the enhancement of gas transport. In addition, steam was found to be the most suitable sweep gas compared with air and oxygen. The exergy analysis showed that a high exergetic efficiency for the SOEC can be achieved at a low operating temperature, high current density, high steam concentration and with many cells. Based on the operating temperature of 1273 K of the SOEC and using oxygen as the sweep gas, the highest energy and exergetic efficiencies of 78.45% and 92.20% were achieved at a current density of 2500 A m^{-2}, a steam concentration of 90% and with the number of cells at 500. Thus, hydrogen production using a SOEC is a promising technology due to the high energy and exergetic efficiencies. However, further detailed investigations are required to justify the possible methods for sustainable hydrogen production to maintain a greener energy generation and utilization.

Acknowledgments

Support from the Chulalongkorn Academic Advancement into Its 2nd Century Project, The Institutional Research Grant (The Thailand Research Fund) (IRG 5780014) and Chulalongkorn University (RES_57_411_21_076) is gratefully acknowledged. K. Im-orb would also like to acknowledge the postdoctoral fellowship from Chulalongkorn University.

Nomenclature

A	cell area (m^2)
B_g	flow permeability (m^2)
$D_{H_2-H_2O}$	molecular diffusion coefficient ($m^2\ s^{-1}$)
$D^{eff}_{H_2O}$	effective diffusion coefficient of steam ($m^2\ s^{-1}$)
$D_{H_2O,k}$	Knudsen diffusion coefficient ($m^2\ s^{-1}$)
d_a	thickness of the anode (m)
d_c	thickness of the cathode (m)
E	equilibrium cell voltage (V)
E^0	standard potential (V)
$E_{act,i}$	activation energy of the cathode (i = c) and anode (i = a) (J $mol^{-1}\ K^{-1}$)
$\dot{E}x_d$	exergy destruction (W)
$\dot{E}x_{in}$	exergy of inlet stream (J mol^{-1})
$\dot{E}x_Q$	exergy of thermal energy (W)

$\dot{E}x_w$	exergy of work (W)
ex_{ch}	specific chemical exergy (J mol^{-1})
$ex_{ch,i0}$	standard chemical exergy of component i (J mol^{-1})
ex	specific exergies (J mol^{-1})
ex_{ph}	specific physical exergy (J mol^{-1})
F	Faraday's constant (C mol^{-1})
h and h_0	enthalpies at the considered and reference environmental states (J mol^{-1})
I	electrical current (A)
J	current density (A m^{-2})
$J_{0,i}$	exchange current density at the cathode (i = c) and anode (i = a) (A m^{-2})
L	thickness of the electrolyte (m)
LHV	lower heating value (J mol^{-1})
M_{H_2}	molar mass of hydrogen (g mol^{-1})
M_{H_2O}	molar mass of steam (g mol^{-1})
N_{cell}	number of cells (−)
$\dot{N}_{H_2,out}$	molar flow rate of the hydrogen product (mol s^{-1})
$\dot{N}_{H_2O}$	molar flow rate of the steam feed (mol s^{-1})
n	electrode porosity (−)
n_e	number of electron (−)
$\dot{n}$	molar flow rate (mol s^{-1})
np	number of inlet streams (−)
nQ	number of heat streams (−)
nr	number of outlet streams (−)
P	operating pressure (kPa)
P_i	partial pressures of component i (kPa)
Q	heat required for the system (W)
Q_E	external heat (W)
Q_{loss}	energy loss (W)
Q_{ovp}	overpotential heat (W)
Q_r	heat required for the reaction (W)
Q_{swg}	sweep gas heat (W)
Q_T	total energy required for the SOEC operation (W)
R	universal gas constant (J mol^{-1} K^{-1})
r	average electrode pore radius (m)
s and s_0	entropies at the considered and reference environmental states (J mol^{-1} K^{-1})
T	cell temperature (K)
T^*	dimensionless temperature (−)
T_0	reference temperature (K)
U_f	utilization factor (−)
V	cell voltage (V)
W	power (W)
$\dot{W}$	shaft work (W)
W_{elec}	SOEC electrical power (W)
y_j	content of component j (−)

Greek symbols

$\frac{\varepsilon_{H_2O}}{K}$ and $\frac{\varepsilon_{H_2}}{K}$	Lennard-Jones potentials of steam and hydrogen (K)
$\eta_{act,a}$, $\eta_{act,c}$	activation overpotentials of the anode and cathode (V)
$\eta_{conc,a}$, $\eta_{conc,c}$	concentration overpotentials of the anode and cathode (V)
η_{en}	energy efficiency (−)
η_{ex}	exergetic efficiency (−)
η_{ohm}	ohmic overpotential (V)
γ_i	pre-exponential factor of the cathode (i = c) and anode (i = a) (A m^{-2})
μ	dynamic viscosity (kg m^{-1} s^{-1})
Ω_D	dimensionless diffusion collision integral (−)
σ_{H_2O} and σ_{H_2}	collision diameters of steam and hydrogen (m)
ξ	electrode tortuosity (−)

References

Angeli, S.D., Monteleone, G., Giaconia, A., Lemonidou, A.A., 2014. State-of-the-art catalysts for CH_4 steam reforming at low temperature. Int. J. Hydrogen Energy 39, 1979–1997.

Authayanun, S., Wiyaratn, W., Assabumrungrat, S., Arpornwichanop, A., 2013. Theoretical analysis of a glycerol reforming and high-temperature PEMFC integrated system: hydrogen production and system efficiency. Fuel 105, 345–352.

Balta, M., Kizilkan, O., Yilmaz, F., 2016. Energy and exergy analyses of integrated hydrogen production system using high temperature steam electrolysis. Int. J. Hydrogen Energy 41, 8032–8041.

Bayat, M., Dehghani, Z., Rahimpour, M.R., 2014. Membrane/sorption-enhanced methanol synthesis process: dynamic simulation and optimization. J. Indus. Eng. Chem. 20, 3256–3269.

Dincer, I., Rosen, M.A., 2012. Exergy: Energy, Environment and Sustainable Development. Elsevier Science.

Dutta, S., 2014. A review on production, storage of hydrogen and its utilization as an energy resource. J. Indus. Eng. Chem. 20, 1148–1156.

Fan, J., Zhu, L., Jiang, P., Li, L., Liu, H., 2016. Comparative exergy analysis of chemical looping combustion thermally coupled and conventional steam methane reforming for hydrogen production. J. Clean. Prod. 131, 247–258.

Ghannadzadeh, A., Thery-Hetreux, R., Baudouin, O., Baudet, P., Floquet, P., Joulia, X., 2012. General methodology for exergy balance in ProSimPlus® process simulator. Energy 44, 38–59.

Gundersen, T., 2009. An Introduction to the Concept of Exergy and Energy Quality. Department of Energy and Process Engineering, Norwegian University of Science and Technology. Trondheim, Norway, Version, 3.

Hajjaji, N., Pons, M., Houas, A., Renaudin, V., 2012. Exergy analysis: an efficient tool for understanding and improving hydrogen production via the steam methane reforming process. Energy Policy 42, 392–399.

He, H., Chen, A., Chang, M., Ma, L., Li, C., 2013. A feasible hydrogen evolution process of water electrolysis assisted by TiO_2 nanotube photocatalysis. J. Indus. Eng. Chem. 19, 1112–1116.

Iribarren, D., Susmozas, A., Petrakopoulou, F., Dufour, J., 2014. Environmental and exergetic evaluation of hydrogen production via lignocellulosic biomass gasification. J. Clean. Prod. 69, 165–175.

Kim, S.J., Kim, K.J., Choi, G.M., 2015. A novel solid oxide electrolysis cell (SOEC) to separate anodic from cathodic polarization under high electrolysis current. Int. J. Hydrogen Energy 40, 9032–9038.

Li, Q., Zheng, Y., Guan, W., Jin, L., Xu, C., Wang, W.G., 2014. Achieving high-efficiency hydrogen production using planar solid-oxide electrolysis stacks. Int. J. Hydrogen Energy 39, 10833–10842.

Mahmood, A., Bano, S., Yu, J.H., Lee, K.H., 2015. High-performance solid oxide electrolysis cell based on ScSZ/GDC (scandia-stabilized zirconia/gadolinium-doped ceria) bi-layered electrolyte and LSCF (lanthanum strontium cobalt ferrite) oxygen electrode. Energy 90, 344–350.

Mikulčić, H., Klemeš, J.J., Vujanović, M., Urbaniec, K., Duić, N., 2016. Reducing greenhouse gasses emissions by fostering the deployment of alternative raw materials and energy sources in the cleaner cement manufacturing process. J. Clean. Prod. 136, 119–132.

Millet, P., Grigoriev, S., 2013. Water Electrolysis Technologies. Renewable Hydrogen Technologies. Elsevier.

Menon, V., Janardhanan, V.M., Deutschmann, O., 2014. A mathematical model to analyze solid oxide electrolyzer cells (SOECs) for hydrogen production. Chem. Eng. Sci. 110, 83–93.

Momma, A., Kato, T., Kaga, Y., Nagata, S., 1997. Polarization behavior of high temperature solid oxide electrolysis cells (SOEC). Nippon. seramikkusu kyokai gakujutsu ronbunshi 105, 369–373.

Ni, M., Leung, M.K.H., Leung, D.Y.C., 2006. A modeling study on concentration overpotentials of a reversible solid oxide fuel cell. J. Power Sources 163, 460–466.

Ni, M., Leung, M.K.H., Leung, D.Y.C., 2007. Parametric study of solid oxide steam electrolyzer for hydrogen production. Int. J. Hydrogen Energy 32, 2305–2313.

Palm, E., Nilsson, L., Åhman, M., 2016. Electricity-based plastics and their potential demand for electricity and carbon dioxide. J. Clean. Prod. 129, 548–555.

Perna, A., Minutillo, M., Jannelli, E., 2016. Hydrogen from intermittent renewable energy sources as gasification medium in integrated waste gasification combined cycle power plants: a performance comparison. Energy 94, 457–465.

Pozzo, M., Lanzini, A., Santarelli, M., 2015. Enhanced biomass-to-liquid (BTL) conversion process through high temperature co-electrolysis in a solid oxide electrolysis cell (SOEC). Fuel 145, 39–49.

Reid, R.C., Prausnitz, J.M., Poling, B.E., 1987. The Properties of Gases and Liquids. McGraw-Hill, New York.

Shao, L., Wang, S., Qian, J., Ye, X., Wen, T., 2013. Optimization of the electrode-supported tubular solid oxide cells for application on fuel cell and steam electrolysis. Int. J. Hydrogen Energy 38 (11), 4272–4280.

Stempien, J.P., Sun, Q., Chan, S.H., 2013. Performance of power generation extension system based on solid-oxide electrolyzer cells under various design conditions. Energy 55, 647–657.

Sun, S., Shao, Z., Yu, H., Li, G., Yi, B., 2014. Investigations on degradation of the long-term proton exchange membrane water electrolysis stack. J. Power Sources 267, 515–520.

Szargut, J., Morris, D.R., Steward, F.R., 1988. Exergy Analysis of Thermal, Chemical

and Metallurgical Processes. Springer.
Todd, B., Young, J., 2002. Thermodynamic and transport properties of gases for use in solid oxide fuel cell modelling. J. Power Sources 110 (1), 186–200.
Udagawa, J., Aguiar, P., Brandon, N.P., 2008. Hydrogen production through steam electrolysis: control strategies for a cathode-supported intermediate temperature solid oxide electrolysis cell. J. Power Sources 180 (1), 354–364.
Valente, A., Iribarren, D., Dufour, J., 2017. Harmonised life-cycle global warming impact of renewable hydrogen. J. Clean. Prod. 149, 762–772.
Zhang, H., Su, S., Chen, X., Lin, G., Chen, J., 2013. Configuration design and performance optimum analysis of a solar-driven high temperature steam electrolysis system for hydrogen production. Int. J. Hydrogen Energy 38 (11), 4298–4307.
Zhang, W., Croiset, E., Douglas, P., Fowler, M., Entchev, E., 2005. Simulation of a tubular solid oxide fuel cell stack using AspenPlus TM unit operation models. Energy Convers. Manag. 46 (2), 181–196.